Observation of energetic electron confinement in a largely stochastic reversed-field pinch plasma

D. J. Clayton, B. E. Chapman, R. O'Connell, A. F. Almagri, D. R. Burke et al.

Citation: Phys. Plasmas **17**, 012505 (2010); doi: 10.1063/1.3292658
View online: http://dx.doi.org/10.1063/1.3292658
View Table of Contents: http://pop.aip.org/resource/1/PHPAEN/v17/i1
Published by the American Institute of Physics.

Observation of energetic electron confinement in a largely stochastic reversed-field pinch plasma

D. J. Clayton,[1] B. E. Chapman,[1] R. O'Connell,[1] A. F. Almagri,[1] D. R. Burke,[1] C. B. Forest,[1] J. A. Goetz,[1] M. C. Kaufman,[1] F. Bonomo,[2] P. Franz,[2] M. Gobbin,[2] and P. Piovesan[2]
[1]*Department of Physics, University of Wisconsin-Madison, Madison, Wisconsin 53706, USA*
[2]*Consorzio RFX, Euratom-ENEA Association, Corso Stati Uniti, 4 35127 Padova, Italy*

(Received 18 September 2009; accepted 22 December 2009; published online 15 January 2010)

Runaway electrons with energies >100 keV are observed with the appearance of an $m=1$ magnetic island in the core of otherwise stochastic Madison Symmetric Torus [Dexter *et al.*, Fusion Technol. **19**, 131 (1991)] reversed-field-pinch plasmas. The island is associated with the innermost resonant tearing mode, which is usually the largest in the $m=1$ spectrum. The island appears over a range of mode spectra, from those with a weakly dominant mode to those, referred to as quasi single helicity, with a strongly dominant mode. In a stochastic field, the rate of electron loss increases with electron parallel velocity. Hence, high-energy electrons imply a region of reduced stochasticity. The global energy confinement time is about the same as in plasmas without high-energy electrons or an island in the core. Hence, the region of reduced stochasticity must be localized. Within a numerical reconstruction of the magnetic field topology, high-energy electrons are substantially better confined inside the island, relative to the external region. Therefore, it is deduced that the island provides a region of reduced stochasticity and that the high-energy electrons are generated and well confined within this region. © *2010 American Institute of Physics*. [doi:10.1063/1.3292658]

I. INTRODUCTION

The reversed-field pinch (RFP) is characterized by poloidal and toroidal magnetic fields of similar magnitude and by reversal of the toroidal field at the edge relative to its direction in the core.[1] In a standard RFP plasma, $m=1$ tearing modes driven by a current gradient form islands on numerous rational surfaces in the plasma core. These islands generally overlap, producing a stochastic field with rapid Rechester–Rosenbluth-like particle transport.[2,3] In a stochastic field, the rate of radial diffusion is proportional to particle parallel velocity, with the fastest particles exiting the plasma first. By inductively altering the current profile, these tearing modes can be suppressed and stochasticity greatly reduced.[4,5] Particle transport is thereby greatly reduced, and radial diffusion becomes independent of particle velocity.[6] One hallmark of these globally improved confinement plasmas is the generation and confinement of runaway electrons with energies as high as 150 keV. The electrons are accelerated by the toroidal electric field, but to reach such a high energy, the electrons must transit the toroidal circumference more than 30 000 times. While runaway electrons have long been used in other toroidal devices as a means of measuring particle transport,[7–15] historically the large tearing modes present in the RFP have prevented the confinement of these high-energy particles. The accelerating electric field is still present in standard, stochastic RFP plasmas, but electrons in this case are only able to reach about 10 keV before they are lost from the plasma.

Another emerging route to globally improved confinement in the RFP is the single helicity state. The $m=1$ tearing modes in standard plasmas are typically of about the same amplitude, but magnetohydrodynamic simulations have predicted that these modes can evolve spontaneously toward a single helicity state, where one mode, usually that resonant closest to the magnetic axis, grows to very large amplitude, while the other, secondary, $m=1$ mode amplitudes vanish.[16,17] The island associated with the dominant mode thereby produces a nonstochastic helical equilibrium in the RFP core. While pure single helicity has yet to be observed experimentally, the so-called quasi-single-helicity (QSH) mode spectra have been observed in several RFP plasmas.[18–24] In QSH spectra, the secondary modes do not vanish but often become smaller. In the RFX, RFX-mod, and Madison Symmetric Torus (MST) RFP devices, soft-x-ray tomography reveals increased x-ray emission inside the island structure during QSH, suggesting a local increase in the electron temperature.[18,19,21,23,24] This has been confirmed with Thomson scattering in RFX and RFX-mod,[18,19,24] but there is not yet a robust temperature increase observed in MST. Most recently in RFX-mod, the dominant mode during QSH reached an amplitude large enough that the island enveloped the plasma's magnetic axis. This resulted in a substantially broader region of increased temperature and produced a several-fold improvement in global energy confinement.[25] Both the measured temperature increase and modeling of the magnetic topology during QSH imply reduced stochasticity and energy transport within the dominant magnetic island. However, there is as yet little experimental information concerning particle transport within the island.

In this paper, we describe data from MST from which we deduce that within a single island in the plasma core, both stochasticity and particle transport are indeed reduced. The evidence for this is the emergence of high-energy runaway electrons in plasmas with an island in the core but

without global confinement improvement. This is the first such observation in the RFP. That global confinement is not improved implies a localized region of reduced stochasticity. Reconstruction of the magnetic field topology and examination of the trajectory of high-energy test particles demonstrates both reduced stochasticity and reduced particle transport within the island. These observations include a variety of $m=1$ mode spectra, ranging from QSH to cases where the innermost-resonant tearing mode is only weakly dominant. This is the first measurement of locally improved particle confinement in QSH plasmas.

Particle transport within an island has previously been studied in the tokamak. Experiments performed on the TEXTOR tokamak have shown that magnetic islands can confine runaway electrons within an otherwise stochastic plasma.[13] In TEXTOR discharges with an electron density less than 10^{19} m^{-3}, runaways with energies up to 30 MeV emerged. Following injection of a deuterium pellet, large magnetic fluctuations developed, and field lines became stochastic. Runaway electrons were rapidly lost to the wall, with the exception of those residing within a remnant $m=2$, $n=1$ island. Within this island, runaway electrons remained well confined, forming a narrow helical beam of high-energy electrons within the otherwise stochastic plasma. The helical beam lasted for more than 0.6 s. While this experimental result supports the notion that an island embedded in an otherwise stochastic field can exhibit good confinement properties, it differs from the plasma conditions presented in this paper in that the tokamak plasma began in a nonstochastic state. In the RFP plasmas described here, the island emerges spontaneously within a stochastic field.

II. EXPERIMENTAL APPARATUS

These studies were performed on the MST, which produces a RFP plasma with a major radius of 1.5 m and a minor radius of 0.5 m.[26] In the plasmas studied here, the toroidal plasma current was about 400 kA with a line-averaged electron density of about 5×10^{18} m^{-3}. Magnetic fluctuation amplitudes are measured with a toroidal array of 32 poloidal and 32 toroidal magnetic field pickup coils mounted at the plasma boundary.

The high-energy runaway electrons in these plasmas emerge due in part to the relatively low density and relatively strong toroidal electric field of about 1.5 V/m in the plasma core. The electrons emit hard-x-ray photons as bremsstrahlung, which can be detected and used to infer the energy distribution of runaways throughout the plasma.[8,14,27] Each photon's energy is some fraction of the kinetic energy of the electron from which the photon is emitted. These photons are diagnosed with an array of 16 CdZnTe solid-state hard-x-ray (hxr) detectors, following the design of a similar array on TORE SUPRA.[27] Each detector is capable of recording individual x rays with energies from 10–300 keV.[28] Hard x rays are a convenient diagnostic tool since there are no other significant sources of radiation above 10 keV in MST. As illustrated in Fig. 1, the detectors are placed along an array of portholes that provide coverage of most of the poloidal cross section. The spacing between chords is about 5 cm. Each

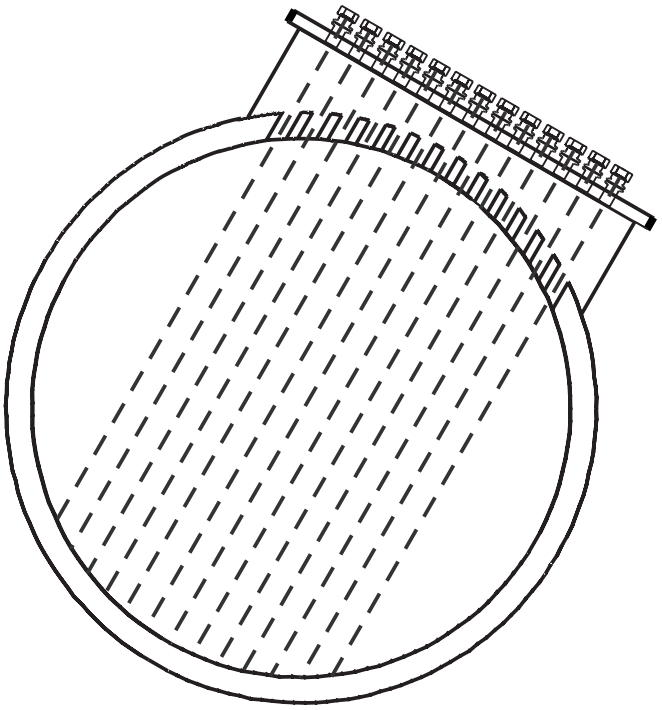

FIG. 1. Poloidal cross section of MST showing placement of CdZnTe hard-x-ray detectors, providing a radial resolution of about 5 cm. The lines of sight are shown with dashed lines. A total of 13 ports is available.

detector is mounted above a 0.4 mm aluminum window that strongly attenuates lower energy photons. Lead apertures of various size are placed between the window and detector to maximize the measured flux while minimizing pulse pileup. The detector housing is surrounded by lead shielding to block high-energy x rays arriving from outside the viewing chord.

The signal from each $10\times10\times2$ mm^3 detector runs first through a current-to-voltage amplifier and then through a shaping amplifier that produces a Gaussian pulse with an amplitude proportional to x-ray energy and a temporal half width of about $1\mu s$. This signal is digitized at 10 MHz, and the data are then processed. Gaussians are fitted to each pulse to remove noise and resolve pileup, and the pulse heights are converted to x-ray energy via calibration with a known x-ray source. By binning x-ray pulses over short time windows, this system allows for measurement of time-resolved energy spectra.

Soft-x-ray (sxr) tomography is used to detect the presence of the central magnetic island. Tomographic data are gathered with four x-ray cameras at the same toroidal angle but at different poloidal angles.[23] Each camera is comprised of an array of silicon photodiodes shielded by an aluminum housing with a pinhole covered with a beryllium filter, providing a total of 74 viewing chords.[29] The brightness measured by the 74 chords is inverted, providing a two-dimensional (2D) profile of soft-x-ray emissivity. This inversion reveals nonaxisymmetric features in the plasma, such as magnetic islands.[23] X-ray emission has for several decades been used to monitor the dynamics of tearing modes in the RFP.[30,31]

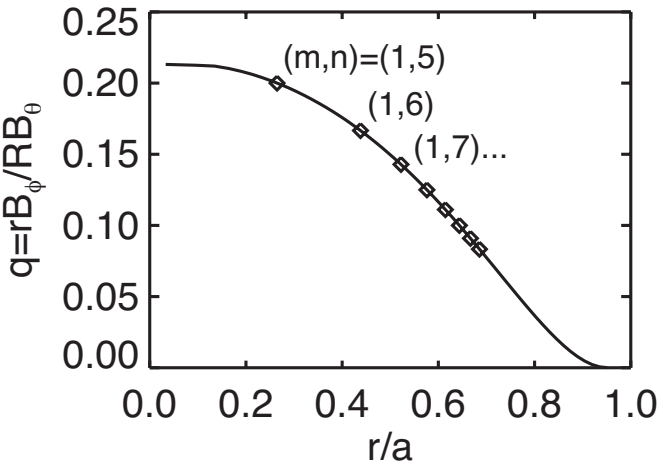

FIG. 2. Safety factor profile from nonreversed discharges.

III. EXPERIMENTAL RESULTS

The measurements described herein were made in discharge conditions that in MST favor the appearance of QSH mode spectra. In addition to the parameters described in Sec. II, another important condition is zero toroidal magnetic field at the plasma boundary, i.e., nonreversed plasmas. The safety factor or q profile for such a plasma is shown in Fig. 2. The equilibrium is distinguished by $q=0$ at the boundary. Also note that the innermost resonant $m=1$ mode has $n=5$. This is usually the dominant mode.

From a typical nonreversed discharge, we display in Fig. 3 the temporal evolution of the central line-integrated hxr flux, two of the $m=1$ mode amplitudes, the so-called spectral spread, and the toroidal plasma current. The spectral spread,

$$N_S = \left[\sum_n \left(\frac{b^2_{\theta,(1,n)}}{\Sigma_n b^2_{\theta,(1,n)}} \right)^2 \right]^{-1}, \quad (1)$$

where the summation is from $n=5-14$ in this analysis. N_S essentially reflects the number of $m=1$ modes of significant amplitude or the degree of spectral peaking.[32] Pure single helicity mode spectra have $N_S=1$. For MST plasmas, QSH mode spectra have historically (and somewhat arbitrarily) been identified by $N_S<2$.

The hxr flux in Fig. 3 is somewhat correlated with the behavior of the $m=1$ modes. Early in time, as the toroidal current is ramping up, the dominant $n=5$ mode exhibits several periods during which it grows and then drops. The hxr flux shows roughly the same behavior. Later in time, after the toroidal current rise phase, there are two periods during which the $n=5$ exhibits large amplitude for sustained periods. The width of the corresponding island, which is proportional to the square root of the mode amplitude, is also large. At the same time, the $n=6$ mode as well as modes with $n>6$ remain relatively small. Because of the very large $n=5$ amplitude, N_S approaches 1 during these periods.

Leading up to 30 ms, the hxr flux grows, with a peak photon energy reaching >100 keV. This energy is comparable to that observed in discharges where the current profile is modified and stochasticity is reduced over much of the plasma.[6] At 30 ms, the $n=5$ mode amplitude drops suddenly,

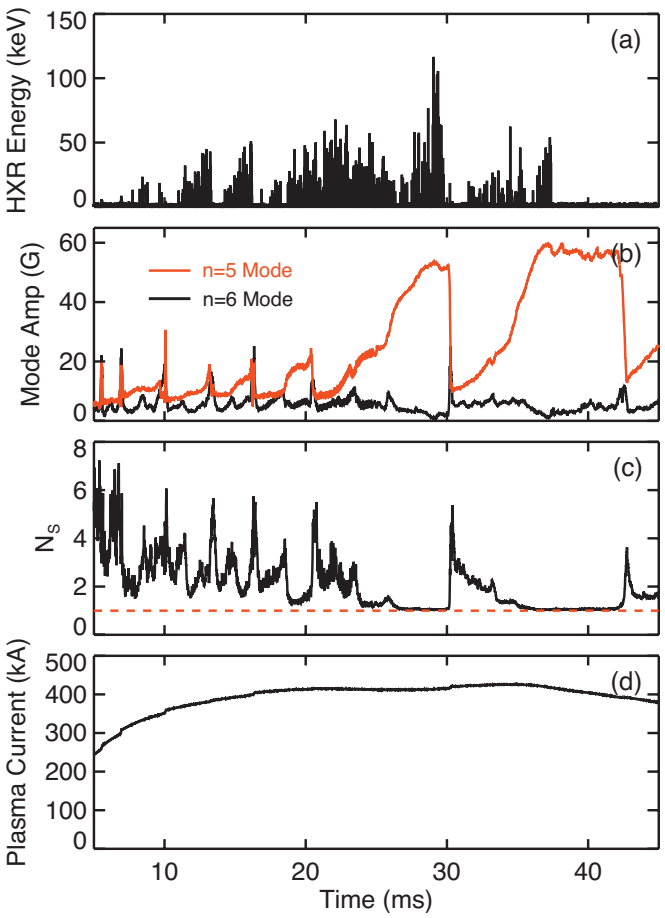

FIG. 3. (Color) In a nonreversed discharge, temporal evolution of (a) the hard-x-ray counts from a central chord, (b) amplitudes of two $m=1$ modes, (c) the spectral spread, defined in the text, and (d) the toroidal plasma current. Each hard-x-ray spike represents a measured photon. The red dashed line in (c) shows for reference the lower bound on the spectral spread. Shot 1061013015.

with a corresponding increase in the amplitudes of the $n\geq 6$ modes. This results in elimination of the hxr flux. Following 30 ms, the $n=5$ mode grows again, with a corresponding re-emergence of the hxr flux. However, shortly after the $n=5$ mode amplitude reaches its peak, the hxr flux vanishes once again.

It is clear from Fig. 3 that N_S and hxr flux are only loosely correlated. However, on average the hxr flux is largest when N_S is small. This is illustrated in Fig. 4, which is based on an average of similar discharges. The hxr flux is largest for values of N_S usually associated with QSH, but there is finite flux for N_S up to 7, corresponding to a fairly broad $m=1$ spectrum. The data in Figs. 3 and 4 reveal that the magnetic mode spectrum is not always useful as a predictor of the presence of hxr flux. A much better predictor is the presence of an island in the plasma core as indicated by sxr tomography.

To illustrate this, in Fig. 5 we zoom in on some of the data shown in Fig. 3. In addition, at the top of the figure, we include sxr emissivity measured across a portion of the poloidal plasma cross section. The oscillating pattern in the sxr data corresponds to an $n=5$ island rotating about the magnetic axis of the plasma, located at about 1.56 m. There is a

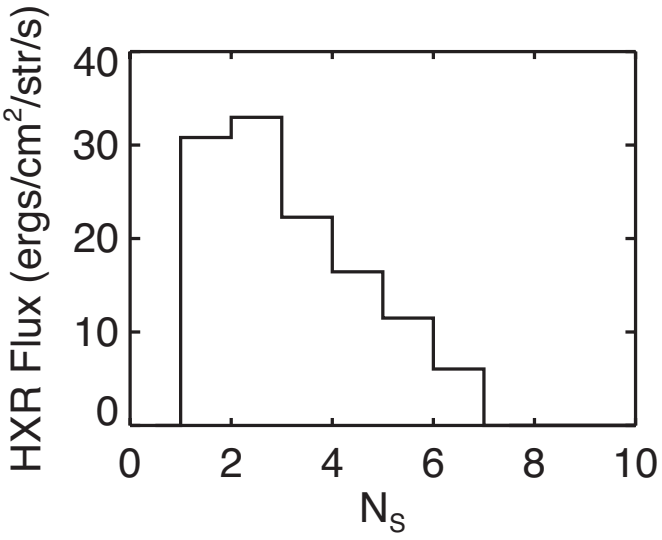

FIG. 4. Dependence of hard-x-ray energy flux on spectral spread. Hard x rays with energies ranging from 10 to 150 keV are included. Histogram results from an average over several discharges similar to that in Fig. 3.

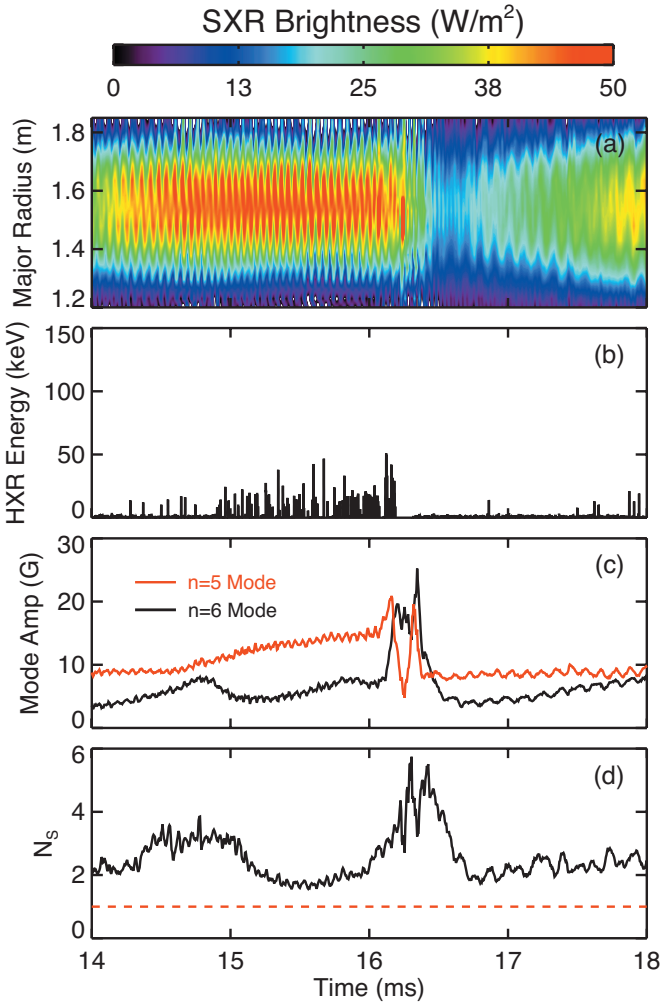

FIG. 5. (Color) Zooming in on data from the discharge in Fig. 3: (a) sxr emission over the plasma cross section, (b) hxr counts, (c) amplitudes of two $m=1$ modes, and (d) the spectral spread.

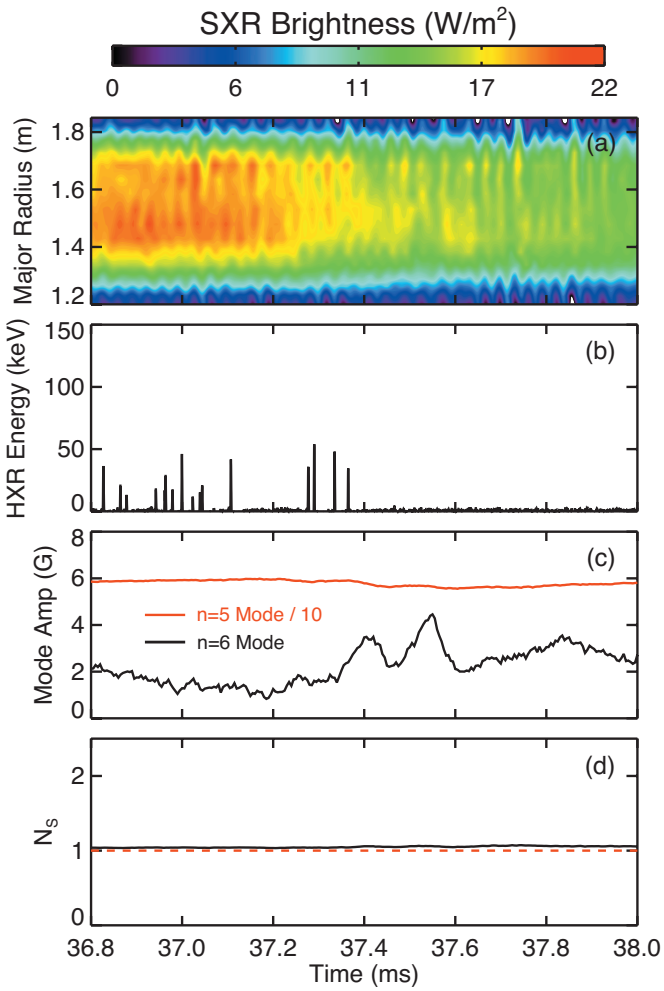

FIG. 6. (Color) Zooming in again on data from the discharge in Fig. 3: (a) sxr emission over the plasma cross section, with a different brightness color mapping relative to Fig. 5, (b) hxr counts, (c) amplitudes of two $m=1$ modes, with the dominant mode scaled down by a factor of 10, and (d) the spectral spread.

clear correlation between the presence of the sxr island structure and the hxr flux. After 16.2 ms, the sxr island is disrupted for a short time as the $n=5$ amplitude drops and the $n=6$ amplitude rises, but the island is later restored along with the hxr flux. These data reveal not only a correlation between sxr structure and hxr emission, but they also reveal that a sxr structure (an island) can exist for $N_S>2$.

In Fig. 6 we zoom in once again on data from the discharge in Fig. 3, and again add sxr emissivity. Now, however, we look late in time at the period during which the $n=5$ mode reaches a large amplitude and saturates, and hxr emission vanishes. Note that after 38 ms, the toroidal current begins to ramp down, and the electric field is no longer strong enough to generate new runaway electrons. This figure once again demonstrates the correlation between the sxr structure and hxr emission. Hard-x-ray emission vanishes when the hot island disappears, although a cooler island remnant may remain. It also demonstrates again that N_S is not a good predictor of either the sxr structure or hxr emission. Even with N_S very close to 1, its minimum possible value, there need not be a sxr structure in the plasma core. This

TABLE I. Global energy confinement times for nonreversed and reversed MST plasmas at two different line-averaged electron densities and a toroidal plasma current of 400 kA. Hard-x-ray emission is observed only in the nonreversed, low-density discharge.

	$n_e=0.5\times10^{19}$ m^{-3}	$n_e=1.0\times10^{19}$ m^{-3}
Nonreversed	1.1 ms	1.5 ms
Reversed	0.7 ms	1.0 ms

figure also suggests a possible explanation, based on the behavior of the $n=6$ and other secondary modes, for the disappearance of the sxr structure and hxr emission. We revisit this topic in Sec. V.

Thus far we have demonstrated that the emergence of high-energy runaway electrons, requiring reduced stochasticity in the plasma, is well correlated with the presence of an island in the core. This is consistent with, but does not prove, the thesis that the runaway electrons are largely generated within the island. However, examination of the global energy confinement time and computational modeling further support the thesis.

Table I contains measurements of the global energy confinement time in MST in nonreversed and normal, reversed plasmas at two different densities. The energy confinement time is the ratio of the volume-integrated stored thermal energy to the volume-integrated Ohmic input power. The nonreversed, low-density case is the only one of the four discharges that exhibits an island. It is also the only case with a measurable hxr emission. All four cases have roughly the same 1 ms confinement time that is the norm for plasmas with a fully stochastic magnetic topology in the core. The energy confinement time increases tenfold when the current profile is suitably modified, and stochasticity is reduced in the core. The fact that the global confinement time in the plasmas examined here is only 1 ms requires that the region of reduced stochasticity and runaway electron generation be localized to a relatively small volume, as is the case with an island in the core.

Before turning to the computational results, we close this section with a more in-depth examination of the hxr data. Given that the core island is apparent in 2D sxr emission, it is natural to look for a similar signature in hxr data, with the premise that hxr emission might also be stronger within the island than without. Unfortunately, the hxr data are inconclusive, but they are instructive. In Fig. 7 is the hxr flux from a single detector in the radial array. This detector was chosen such that the rotating island regularly passes in and out of the detector's line of sight. The flux in Fig. 7 is plotted versus the location of the island's O-point in the poloidal plane. If hxr emission is enhanced within the island, one could reasonably expect the flux to depend on the island's position, but according to Fig. 7, it does not. The other detectors provide the same result. This lack of island phase dependence may be due to substantial additional emission outside the island, both within the plasma and at the plasma-facing wall.

The case for hxr emission from the bulk plasma outside the island and from the plasma-facing wall is established by first examining the radial profile of hxr flux. In Fig. 8 is the

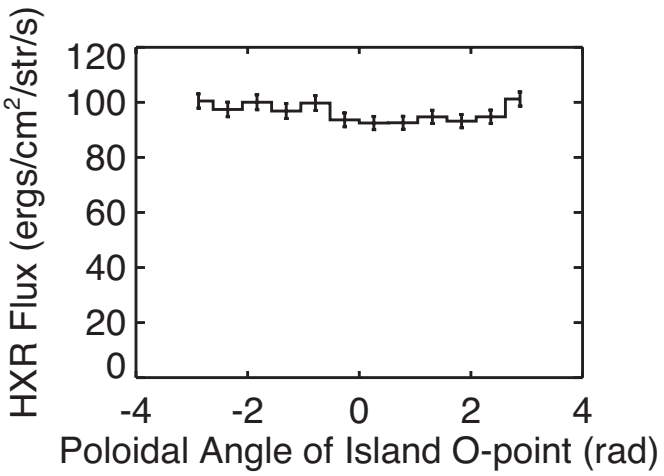

FIG. 7. HXR flux from 10 to 150 keV vs the poloidal angle of the island O-point at the toroidal angle of the detector.

radial profile of hxr flux for a typical nonreversed plasma as well as a plasma with global tearing mode reduction. Each datum is a line-integrated flux, and the points near $r/a=0$ have the longest path lengths. The island in the nonreversed plasma resides well inside $|r/a|=0.6$. The profile maxima are shifted outward, consistent with the usual outward shift of the magnetic axis. The profiles also have an asymmetry due to the anisotropic angular distribution of relativistic bremsstrahlung. The profile from the reduced tearing mode plasma is peaked in the core region, where flux surfaces are restored and temperatures are the highest. By comparison, the nonreversed case shows a broader profile, implying a larger contribution from the plasma outside of $|r/a|=0.6$ and/or from target emission at the plasma-facing wall. Also of note is that the two profiles are of similar magnitude. Although the runaway electrons in the nonreversed case are necessarily generated in a smaller volume than in the reduced-tearing case, the loop voltage or accelerating electric field is roughly three

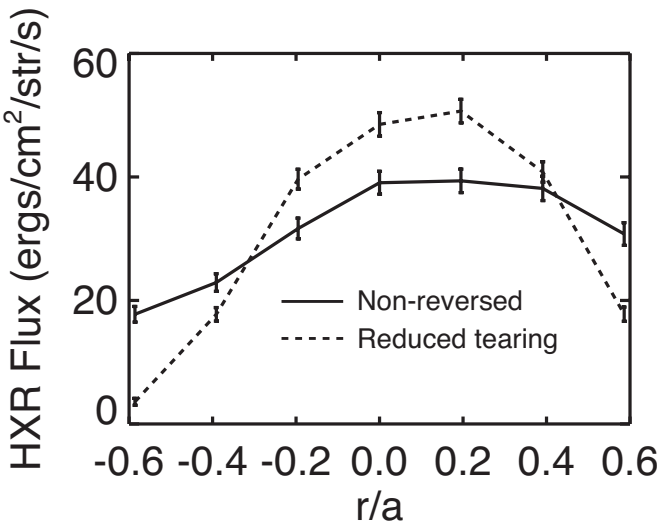

FIG. 8. Including photon energies ranging from 10 to 150 keV, line-integrated hxr flux profiles from a nonreversed plasma discharge and a discharge with a modified current profile and reduced tearing.

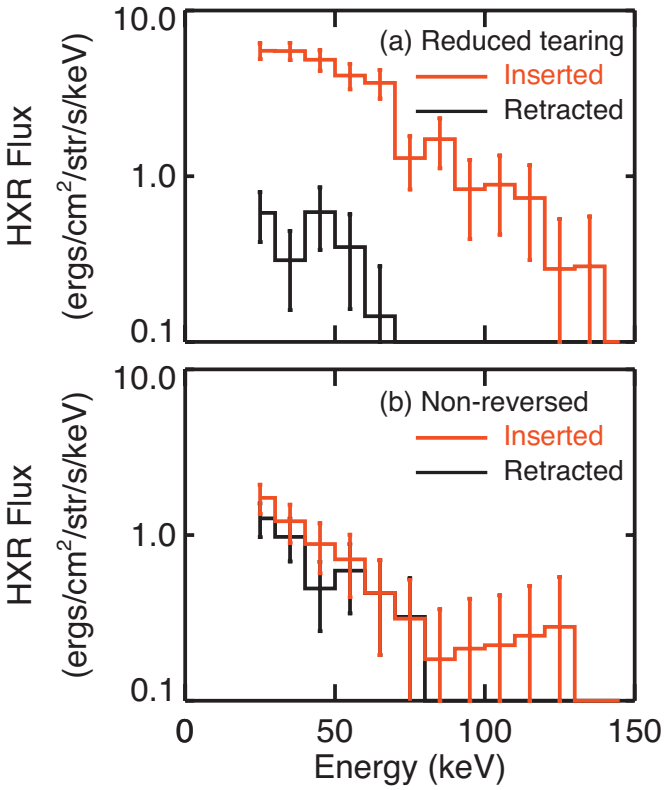

FIG. 9. (Color) HXR energy spectra from a detector viewing an inserted target probe and the same detector viewing the fully retracted probe in (a) plasmas with current profile modification and reduced tearing modes in the core and (b) nonreversed plasmas.

times larger in the nonreversed case,[33] thereby generating a larger number of high-energy electrons more rapidly.

In several toroidal devices, hard-x-ray flux has been produced from runaways striking plasma limiters.[7,9,12] Evidence for similar emission at the plasma-facing wall in MST is provided by monitoring an insertable target probe, similar to the probes used in the ASDEK tokamak to measure the runaway population at a point near the plasma boundary.[11] On MST, a molybdenum-tipped probe was mounted on a port directly across from one of the hxr detectors and inserted 0.05 m into the plasma. The signal from this detector is compared to that obtained by the same detector when the probe was retracted. Data were gathered in nonreversed plasmas and in plasmas with tearing mode reduction. Note that the flux measured by the other detectors was used as a control in these measurements. In each of the two sets of plasma, the flux measured by the other detectors exhibited little shot-to-shot variation and remained unchanged when the probe was inserted.

In Fig. 9(a) are hxr flux energy spectra during tearing mode reduction. When the target probe is inserted 0.05 m into the plasma, the measured emission jumps by more than an order of magnitude. Runaway electrons that strike the solid target emit large amounts of bremsstrahlung, thus the large increase in emission demonstrates that there is a population of runaway electrons reaching the edge of the plasma. This is in sharp contrast to nonreversed plasmas, Fig. 9(b). Here, insertion of the probe makes very little difference in the measured flux. These data imply that only a tiny fraction of runaways reach the plasma-facing wall in the nonreversed case. Ruling out significant emission from the wall, the relatively flatter hxr flux profile in Fig. 8 is likely due in large part to spatially diffuse emission throughout the plasma volume.

Assuming that the only region of reduced stochasticity in these plasmas is within the island in the plasma core, one can easily speculate why there are high-energy electrons in the bulk plasma. It requires only finite transport of high-energy electrons across the island separatrix. Once outside the island, these electrons will then wander stochastically throughout the plasma volume, emitting bremsstrahlung along the way. The hxr data are thus incapable of providing the exact location where the electrons are accelerated to high energy. Therefore, we turn to computational modeling.

IV. COMPUTATIONAL RESULTS

With computational modeling of both the magnetic topology and the trajectory of test particles placed in that topology, we find that initially thermal electrons are accelerated to high energy within the island associated with the dominant $n=5$ mode. The computation was performed with ORBIT, a Hamiltonian guiding center code.[34] ORBIT has been used in the recent past to predict the rate of transport of purely thermal electrons and ions in the presence of both fully stochastic and QSH (local reduction in stochasticity) magnetic topologies. The particle loss rate was found to be locally reduced within the island region in the QSH case.[35,36] To simulate the plasmas described in this paper, the magnetic equilibrium is first reconstructed based on toroidal and poloidal field measurements at the MST plasma boundary and a standard RFP equilibrium model. The perturbation to the magnetic topology is calculated in ORBIT based on measurements of the tearing mode amplitudes using MST's toroidal array of magnetic sensing coils. When the $n=5$ mode is dominant in the $m=1$ spectrum, ORBIT predicts the formation of an $n=5$ island embedded in an otherwise stochastic background.

To initialize the test particle simulation, 1000 particles were placed within the island region. These particles had an effective initial temperature of 250 eV with random trajectories. A toroidal electric field of 1.5 V/m was applied. The particle trajectories were then allowed to evolve over about 2 ms. During this evolution, both pitch-angle and slowing-down collisions were included. The results of the simulation are shown in Figs. 10 and 11, which provide complementary views of the data. In Fig. 10 we show the distribution of electron energies, each electron represented by a dot, over the plasma minor radius, represented by poloidal flux. The vertical shaded band represents the width of the $n=5$ island. The highest-energy electrons are located within the island, but there are also electrons well outside the island, consistent with what is expected from the experimental picture laid out in Sec. III. Although there are uncertainties in the experimental data used in the simulation, the largest electron kinetic energies seen in bulk are consistent with the hxr photon energies shown earlier, bearing in mind that only a fraction of

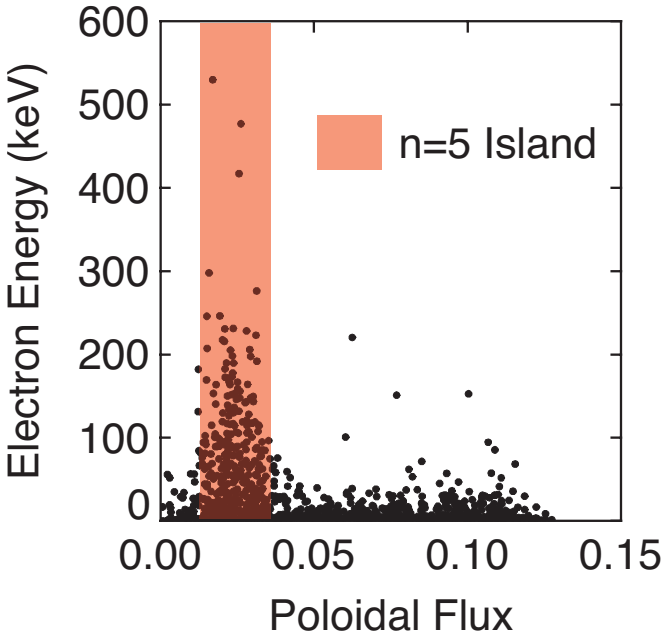

FIG. 10. (Color) From a simulation with the ORBIT code, final radial distribution of test electron energies after acceleration by an electric field. Each dot represents a single electron. The poloidal flux is a proxy for the radial coordinate. Shaded region indicates the width of the $n=5$ island.

the kinetic energy is emitted as radiation. The distribution of electron energies is plotted again in Fig. 11, this time versus poloidal and toroidal angle. Particles with an energy >40 keV are indicated with red dots. Thus, the highest energy particles have an $m=1$, $n=5$ spatial distribution, consistent with their confinement within the $n=5$ island.

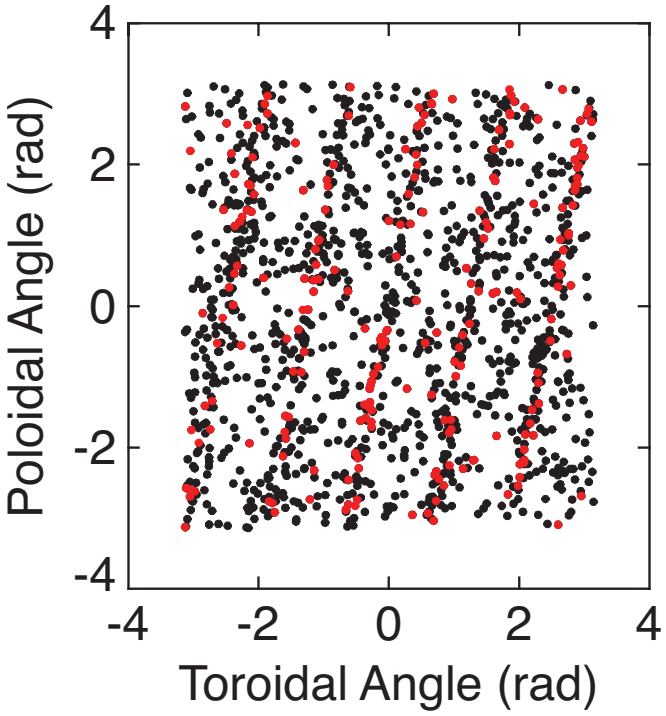

FIG. 11. (Color) Final poloidal and toroidal positions of test electrons from the same simulation as in Fig. 10. Particles with an energy >40 keV indicated with red dots.

In addition to modeling plasmas with a dominant $n=5$ mode, cases were also examined in which all the mode amplitudes were comparable. Such a spectrum occurs just after 16.2 ms in Fig. 5. In such cases, ORBIT predicts a fully stochastic magnetic topology in the plasma core. Test particles deposited in the core undergo acceleration, but their maximum final energy is much lower than with an island present.

V. SUMMARY AND CONCLUSIONS

Hard x rays are emitted from MST plasmas with a magnetic island in the core. These high-energy photons arise from runaway electrons, requiring reduced stochasticity in the plasma. The global energy confinement time in these plasmas is comparable to that in plasmas with no hard-x-ray emission and with a fully stochastic magnetic field in the core. Hence, the region of reduced stochasticity is deduced to be localized to a relatively small volume. In a computational reconstruction of the magnetic field topology, an island emerges in the plasma core associated with the dominant mode. Test electrons placed within this island and undergoing acceleration by a toroidal electric field reach an energy comparable to that observed experimentally, and while the electrons diffuse across the plasma, the highest-energy electrons remain within the island. These results are similar to the previously discussed results from the TEXTOR tokamak, where high-energy runaway electrons can be well confined inside a magnetic island even when the surrounding plasma becomes stochastic. These experimental and computational data lead us to the conclusion that stochasticity is indeed reduced within the island and that particle confinement is improved substantially therein.

We have also shown that the degree of peaking of the $m=1$ mode spectrum is insufficient to determine the presence or absence of an island, or at least a sxr structure, in the core. Even with a very large dominant mode, soft-x-ray tomography reveals that an associated sxr island structure is not always present. The determination of the presence of an island requires internal diagnosis of the plasma. This brings us back to one lingering point from the discussion of Fig. 6. Although the dominant mode is very large in the time window displayed there, the island structure dissipates at one point, and hxr emission ceases. A possible explanation for this is found in the behavior of the secondary modes, represented in that figure by the $n=6$ mode. This secondary mode amplitude increases at the same time the island structure begins to dissipate. Given the large amplitude of the dominant $n=5$ mode, its associated island can overlap the $n=6$ resonant surface. If the $n=6$ mode amplitude becomes sufficiently large, this overlap will bring about stochasticity in that region. The fundamental point is that, as has been noted elsewhere, the formation of a nonstochastic island by a single large mode depends not only on that mode being sufficiently large, but on the secondary modes being sufficiently small.

ACKNOWLEDGMENTS

The authors would like to thank the MST team for their support in this research and the RFX-mod team for their

collaboration. This work was supported by the U.S. Department of Energy cooperative agreement DE-FC02-05ER54814.

[1]H. A. B. Bodin and A. A. Newton, Nucl. Fusion **20**, 1255 (1980).
[2]A. B. Rechester and M. N. Rosenbluth, Phys. Rev. Lett. **40**, 38 (1978).
[3]T. M. Biewer, C. B. Forest, J. K. Anderson, G. Fiskel, B. Hudson, S. C. Prager, J. S. Sarff, J. C. Wright, D. L. Brower, W. X. Ding, and S. D. Terry, Phys. Rev. Lett. **91**, 045004 (2003).
[4]J. S. Sarff, S. A. Hokin, H. Ji, S. C. Prager, and C. R. Sovinec, Phys. Rev. Lett. **72**, 3670 (1994).
[5]B. E. Chapman, J. K. Anderson, T. M. Biewer, D. L. Brower, S. Castillo, P. K. Chattopadhyay, C.-S. Chiang, D. Craig, D. J. Den Hartog, G. Fiksel, P. W. Fontana, C. B. Forest, S. Gerhardt, A. K. Hansen, D. Holly, Y. Jiang, N. E. Lanier, S. C. Prager, J. C. Reardon, and J. S. Sarff, Phys. Rev. Lett. **87**, 205001 (2001).
[6]R. O'Connell, D. J. Den Hartog, C. B. Forest, J. K. Anderson, T. M. Biewer, B. E. Chapman, D. Craig, G. Fiksel, S. C. Prager, J. S. Sarff, and S. D. Terry, Phys. Rev. Lett. **91**, 045002 (2003).
[7]W. Bernstein, F. F. Chen, M. A. Heald, and A. Z. Kranz, Phys. Fluids **1**, 430 (1958).
[8]R. M. Kulsrud, Y.-C. Sun, N. K. Winsor, and H. A. Fallon, Phys. Rev. Lett. **31**, 690 (1973).
[9]S. J. Zweben, D. W. Swain, and H. H. Fleischmann, Nucl. Fusion **18**, 1679 (1978).
[10]H. Knoepfel and D. A. Spong, Nucl. Fusion **19**, 785 (1979).
[11]ASDEX Team, NI Team, O. J. Kwon, P. H. Diamond, F. Wagner, and G. Fussmann, Nucl. Fusion **28**, 1931 (1988).
[12]J. R. Myra, P. J. Catto, A. J. Wootton, R. D. Bengtson, and P. W. Wang, Phys. Fluids B **4**, 2092 (1992).
[13]R. Jaspers, N. J. Lopes Cardozo, K. H. Finken, B. C. Schokker, G. Mank, G. Fuchs, and F. C. Schüller, Phys. Rev. Lett. **72**, 4093 (1994).
[14]B. Esposito, R. Martin Solis, P. van Belle, O. N. Jarvis, F. B. Marcus, G. Sadler, R. Sanchez, B. Fischer, P. Froissard, J. M. Adams, E. Cecil, and N. Watkins, Plasma Phys. Controlled Fusion **38**, 2035 (1996).
[15]I. Entrop, N. J. Lopes Cardozo, R. Jaspers, and K. H. Finken, Plasma Phys. Controlled Fusion **40**, 1513 (1998).
[16]S. Cappello and R. Paccagnella, Phys. Fluids B **4**, 611 (1992).
[17]J. M. Finn, R. Nebel, and C. Bathke, Phys. Fluids B **4**, 1262 (1992).
[18]D. F. Escande, P. Martin, S. Ortolani, A. Buffa, P. Franz, L. Marrelli, E. Martines, G. Spizzo, S. Cappello, A. Murari, R. Pasqualotto, and P. Zanca, Phys. Rev. Lett. **85**, 1662 (2000).
[19]P. Martin, A. Buffa, S. Cappello, F. D'Angelo, D. F. Escande, P. Franz, L. Marrelli, E. Martines, S. Ortolani, G. Spizzo, R. Bilato, T. Bolzonella, S. Costa, A. Murari, R. Paccagnella, R. Pasqualotto, D. Terranova, and P. Zanca, Phys. Plasmas **7**, 1984 (2000).
[20]L. Marrelli, P. Martin, G. Spizzo, P. Franz, B. E. Chapman, D. Craig, J. S. Sarff, T. M. Biewer, S. C. Prager, and J. C. Reardon, Phys. Plasmas **9**, 2868 (2002).
[21]RFX Team, MST Team, EXTRAP T2R Team, TPE-RX Team, P. Martin, L. Marrelli, G. Spizzo, P. Franz, P. Piovesan, I. Predebon, T. Bolzonella, S. Cappello, A. Cravotta, D. F. Escande, L. Frassinetti, S. Ortolani, R. Paccagnella, D. Terranova, B. E. Chapman, D. Craig, S. C. Prager, J. S. Sarff, P. Brunsell, J.-A. Malmberg, J. Drake, Y. Yagi, H. Koguchi, Y. Hirano, R. B. White, C. Sovinec, C. Xiao, R. A. Nebel, and D. D. Schnack, Nucl. Fusion **43**, 1855 (2003).
[22]P. Piovesan, G. Spizzo, Y. Yagi, H. Koguchi, T. Shimada, Y. Hirano, and P. Martin, Phys. Plasmas **11**, 151 (2004).
[23]P. Franz, L. Marrelli, P. Piovesan, I. Predebon, F. Bonomo, L. Frassinetti, P. Martin, G. Spizzo, B. E. Chapman, D. Craig, and J. S. Sarff, Phys. Plasmas **13**, 012510 (2006).
[24]RFX-mod Team, P. Martin, L. Marrelli, A. Alfier, F. Bonomo, D. F. Escande, P. Franz, L. Frassinetti, M. Gobbin, R. Pasqualotto, P. Piovesan, and D. Terranova, Plasma Phys. Controlled Fusion **49**, A177 (2007).
[25]R. Lorenzini, D. Terranova, A. Alfier, P. Innocente, E. Martines, R. Pasqualotto, and P. Zanca, Phys. Rev. Lett. **101**, 025005 (2008).
[26]R. N. Dexter, D. W. Kerst, T. W. Lovell, S. C. Prager, and J. C. Sprott, Fusion Technol. **19**, 131 (1991).
[27]Y. Peysson and F. Imbeaux, Rev. Sci. Instrum. **70**, 3987 (1999).
[28]R. O'Connell, D. J. Den Hartog, C. B. Forest, and R. W. Harvey, Rev. Sci. Instrum. **74**, 2001 (2003).
[29]P. Franz, G. Gadani, R. Pasqualotto, L. Marrelli, P. Martin, G. Spizzo, P. Brunsell, B. E. Chapman, F. Paganucci, P. Rossetti, and C. Xiao, Rev. Sci. Instrum. **74**, 2152 (2003).
[30]G. A. Wurden, Phys. Fluids **27**, 551 (1984).
[31]R. J. Hayden and B. Alper, Plasma Phys. Controlled Fusion **31**, 193 (1989).
[32]Y. L. Ho, D. D. Schnack, P. Nordlund, S. Mazur, H.-E. Satherblom, J. Scheffel, and J. R. Drake, Phys. Plasmas **2**, 3407 (1995).
[33]J. K. Anderson, T. M. Biewer, C. B. Forest, R. O'Connell, S. C. Prager, and J. S. Sarff, Phys. Plasmas **11**, L9 (2004).
[34]R. B. White and M. S. Chance, Phys. Fluids **27**, 2455 (1984).
[35]I. Predebon, L. Marrelli, R. B. White, and P. Martin, Phys. Rev. Lett. **93**, 145001 (2004).
[36]M. Gobbin, L. Marrelli, P. Martin, and R. B. White, Phys. Plasmas **14**, 072305 (2007).